Research Square

Preprints are preliminary reports that have not undergone peer review.
They should not be considered conclusive, used to inform clinical practice,
or referenced by the media as validated information.

Effects of microstructure on reliability of BME-MLCCs

Yunfei He
Chengdu Hongke Electronic Technology Co., Ltd
Qijun Cheng
carexin3@163.com
Chengdu Hongke Electronic Technology Co., Ltd
Fengju Yi
Chengdu Hongke Electronic Technology Co., Ltd
Zengwei Zheng
Chengdu Hongke Electronic Technology Co., Ltd
Qihang Yang
Chengdu Hongke Electronic Technology Co., Ltd

Research Article

Keywords: grinding intensity, microstructure, reliability, BME-MLCC

Posted Date: March 31st, 2026

DOI: https://doi.org/10.21203/rs.3.rs-9197207/v1

License: This work is licensed under a Creative Commons Attribution 4.0 International License.
Read Full License

Additional Declarations: No competing interests reported.

Effects of microstructure on reliability of BME-MLCCs

Yunfei He[1], Qijun Cheng[1]*, Fengju Yi, Zengwei Zheng, Qihang Yang
(Chengdu Hongke Electronic Technology Co., Ltd, Chengdu, China.)
(Correspondence: Qijun Cheng, Email:carexin3@163.com)

Abstract: Five types of base metal multilayer ceramic dielectric capacitors (BME-MLCCs) with distinct microstructure were fabricated by adjusting the grinding intensity. The microstructural characteristics of the ceramics, including micro-morphology, grain size, and pore distribution, were analyzed using a scanning electron microscope (SEM). The impact of the microstructure of the ceramic thin films on the electrical properties and reliability of BME-MLCCs was discussed. The study found that when the grinding was insufficient or excessive, microscopic issues such as non-compactness, unevenness, and pores appeared in the dielectric layer, leading to capacity dispersion, a decline in insulation performance, and reduced reliability. It can thus be seen that grinding intensity serves as the foundation for preparing the dielectric layer, and a high-quality microscopic morphology of the dielectric layer is the key to achieving stable electrical properties and high reliability.

Key word: grinding intensity; microstructure; reliability; BME-MLCC

1 Introduction

In recent years, with the rapid development of the electronic information industry, electronic components towards miniaturization, integration and high performance of the direction of continuous progress [1-3]. As one of the indispensable components in electronic circuits, the demand for multilayer ceramic dielectric capacitors (MLCCs) is increasing day by day [4-5].

However, the traditional precious metal electrode (PME) MLCC due to the use of expensive palladium, platinum and other precious metals as the inner electrode material, resulting in high costs, it is difficult to meet the needs of the modern electronics industry for low-cost, high-performance MLCCs. The base metal multilayer ceramic dielectric capacitors (BME-MLCCs) using nickel (Ni), copper (Cu) and other base metals as the inner electrode significantly reduces the production cost, it has a higher specific capacitance and better frequency characteristics gradually become the mainstream direction of MLCCs development at the same time [6-7].

However, with the higher frequency of usage in harsh environments such as high temperature and high humidity, the reliability of BME-MLCCs is increasingly demanding [8-9]. In BME-MLCCs, porcelain film is used as the key component dielectric layer. Its microstructure such as grain arrangement compactness and porosity will directly affect the dielectric properties, mechanical strength and long-term stability of MLCC, which is decisive for reliability [8,10-13].

For investigating the mechanism of microstructure influence on the reliability of BME-MLCCs. This study has analyzed the electrical properties, mechanical properties and reliability of BME-MLCCs with different grain arrangement compactness, the intrinsic relationship between microstructural densities and reliability is revealed.

2 Methods

2.1 Preparation of porcelain film

Five ceramic films with distinct microstructures were prepared using the batch casting method. Porcelain powder (X7R3000-S3, KCM Company), solvent, homemade binder, and various additives were mixed and ground in a sand mill. The five porcelain slurries obtained were identical except for the number of grinding times (Table 1). After cooling to room temperature, the slurries were applied to a carrier tape using a casting machine and then dried in an oven to form a dielectric porcelain film with a thickness of 5.5 μm.

Table 1 Process parameters of slurry preparation

No.	Grinding time	Grinding media	Size of grinding medium (mm)	Rotate speed (rpm)
S1	10	zirconium ball	0.3	1000
S2	12	zirconium ball	0.3	1000
S3	14	zirconium ball	0.3	1000
S4	16	zirconium ball	0.3	1000
S5	18	zirconium ball	0.3	1000

2.2 Preparation of BME-MLCC

The preparation process for BME-MLCCs is shown in Fig. 1. Five groups of samples (0805-X7R-50V-104) were composed of porcelain films prepared from the above slurries, nickel inner electrodes, and copper terminal electrodes. The green bodies were degassed at 280 °C for 20 h, followed by sintering at 1250 °C for 2 h under a reducing atmosphere (volume ratio 1.2% $H_2/N_2/H_2O$). The process parameters for the five groups of samples were identical except for the different number of grinding times for the porcelain slurry.

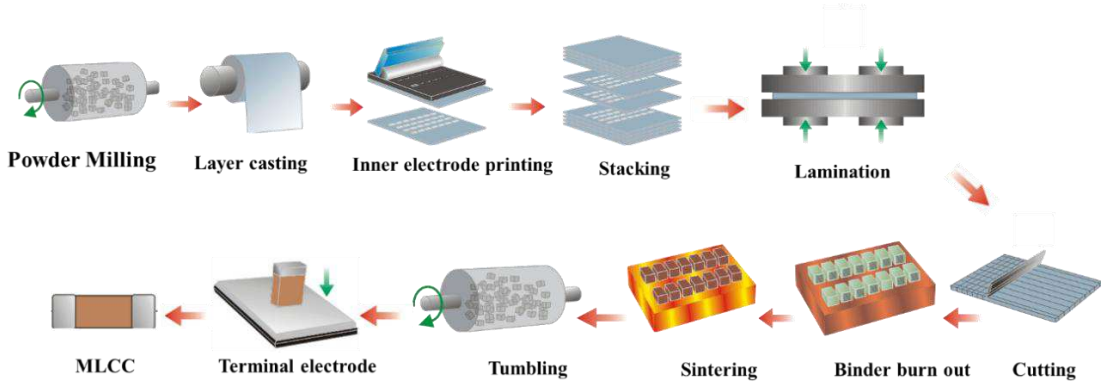


Fig. 1. Schematic diagram of preparation process for BME-MLCC

2.3 Characterization methods

The particle size of the ceramic slurry was determined using a laser particle size analyzer (Malvern Mastersizer 3000). Micrographs of the ceramic film, sample end faces, and inner electrode profiles were observed using a scanning electron microscope (SEM, SU3500, JEOL), and the average size of the end faces was determined using Nano Measurer software. A carbon/sulfur analyzer (HORIBA-EMIA-Pro) was used to detect the amount of residual carbon in the samples. A capacitance analyzer (E4981A) measured the capacitance and dielectric loss of the samples. Breakdown voltage (BDV) was tested using a digital display voltage withstand device (DG-FEJ). Highly Accelerated Life Test (HALT) samples were tested using a test chamber (SPC-T).

3 Result and discussion

3.1 Morphological characterization

Fig. 2 shows the particle size distribution of ceramic slurries S1~S5. The overall particle size of the ceramic slurry gradually decreases with increasing grinding intensity, primarily due to larger particles being continuously broken down into finer ceramic powders under the impact, compression, and shear forces exerted by the grinding media (zirconia balls). The rate of particle size reduction gradually decreases with increasing grinding times, leading to a stabilization of particle size distribution, indicating that larger ceramic powder particles have been sufficiently dispersed without significant agglomeration.

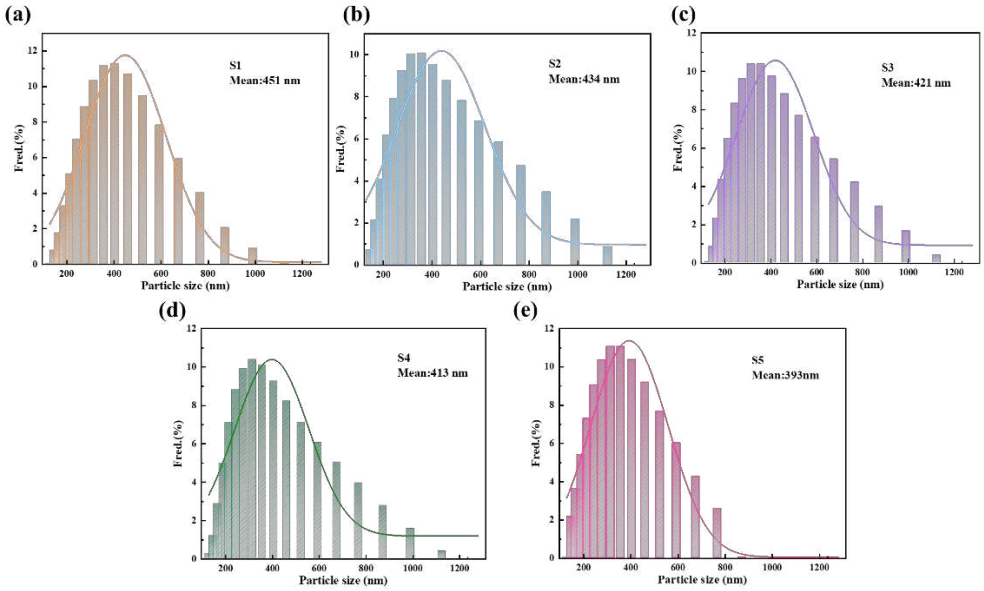


Fig. 2. The ceramic slurry size distribution diagram

Fig. 3(a-e) display the microstructures of ceramic films S1~S5. Initially, the film surface is rough with numerous large-sized particle agglomerates and uneven distribution. After continued grinding, the film surface becomes relatively smooth with a denser structure. However, excessive grinding destroys particle morphology, resulting in a pitted and uneven ceramic film surface with

numerous accumulations and small cracks. Fig. 3(f-j) present the grain size distribution of S1-S5 ceramic films. The grain sizes for samples S1, S2, S3, S4, and S5 were 328 nm, 320 nm, 265 nm, 258 nm, and 244 nm, respectively. As grinding intensity increased, the grain size of the ceramic film tended to decrease gradually, similar to the particle size of the ceramic slurry.

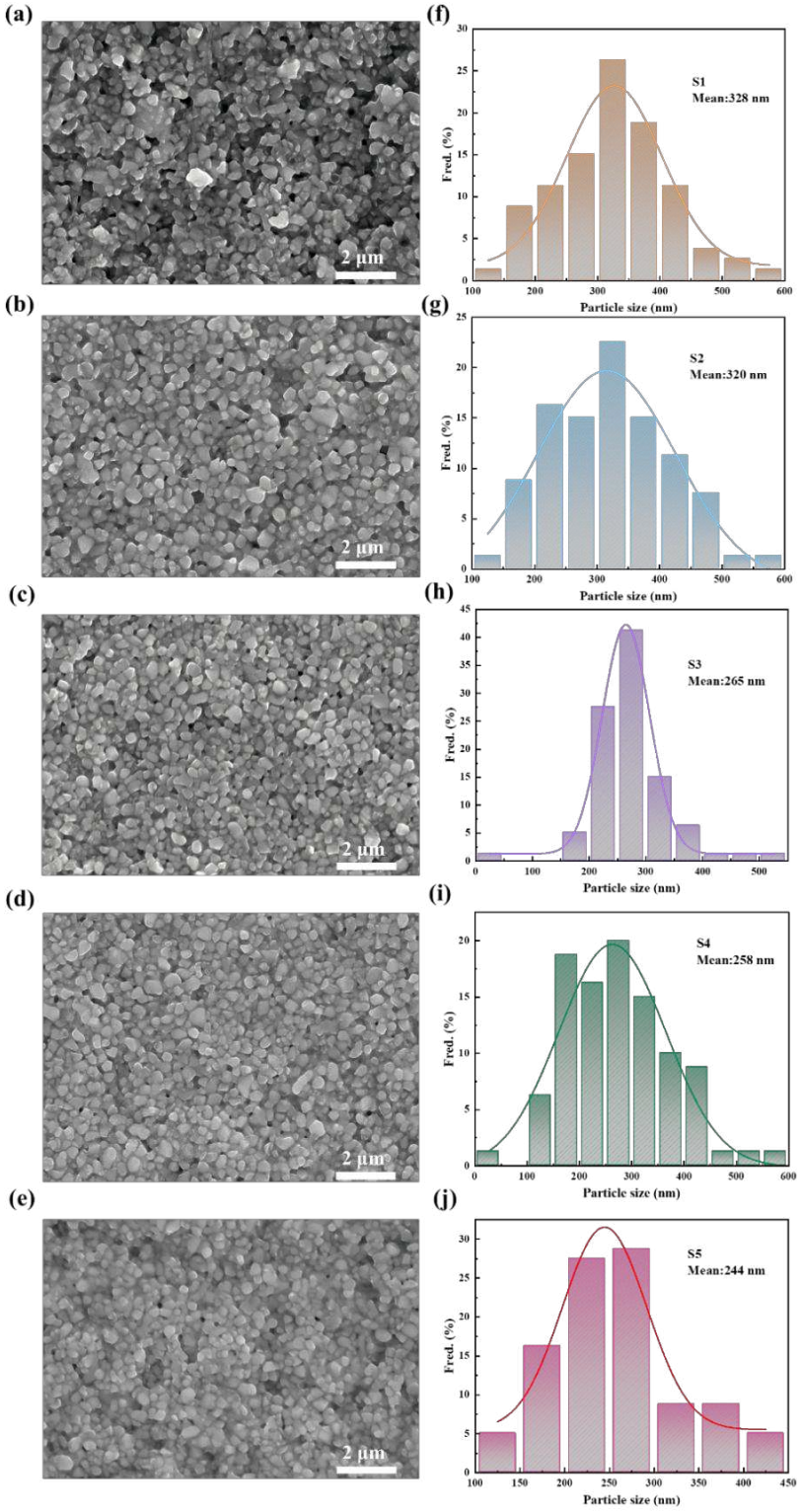


Fig. 3. (a-e) SEM microstructure diagram of porcelain film; (f-j) particle size distribution diagram of porcelain film

Fig. 4(a-e) illustrates the micro-morphologies of the end faces of BME-MLCCs. It was observed that with increasing grinding intensity, the flatness and compactness of the end faces of BME-MLCCs in Groups S1-S4 significantly improved, accompanied by a gradual reduction in voids within the dielectric layers. However, an anomalous pattern emerged in the end-face morphology of BME-MLCCs in Group S5. According to the micro-morphologies of the ceramic films depicted in Fig. 3, the grain sizes of the ceramic films in Groups S1-S5 decreased sequentially. Studies have shown that [14], given a constant dielectric layer thickness, the number of grain boundaries within the dielectric layer progressively increased as the grain size decreased. During the sintering process, the grain boundaries exhibited high reactivity, facilitating the filling of voids by smaller particles and thereby enhancing the compactness of the ceramic body. Nevertheless, excessive grinding intensity led to increased blurriness and disorder at the grain boundaries, ultimately resulting in a less compact ceramic body with the re-emergence of voids.

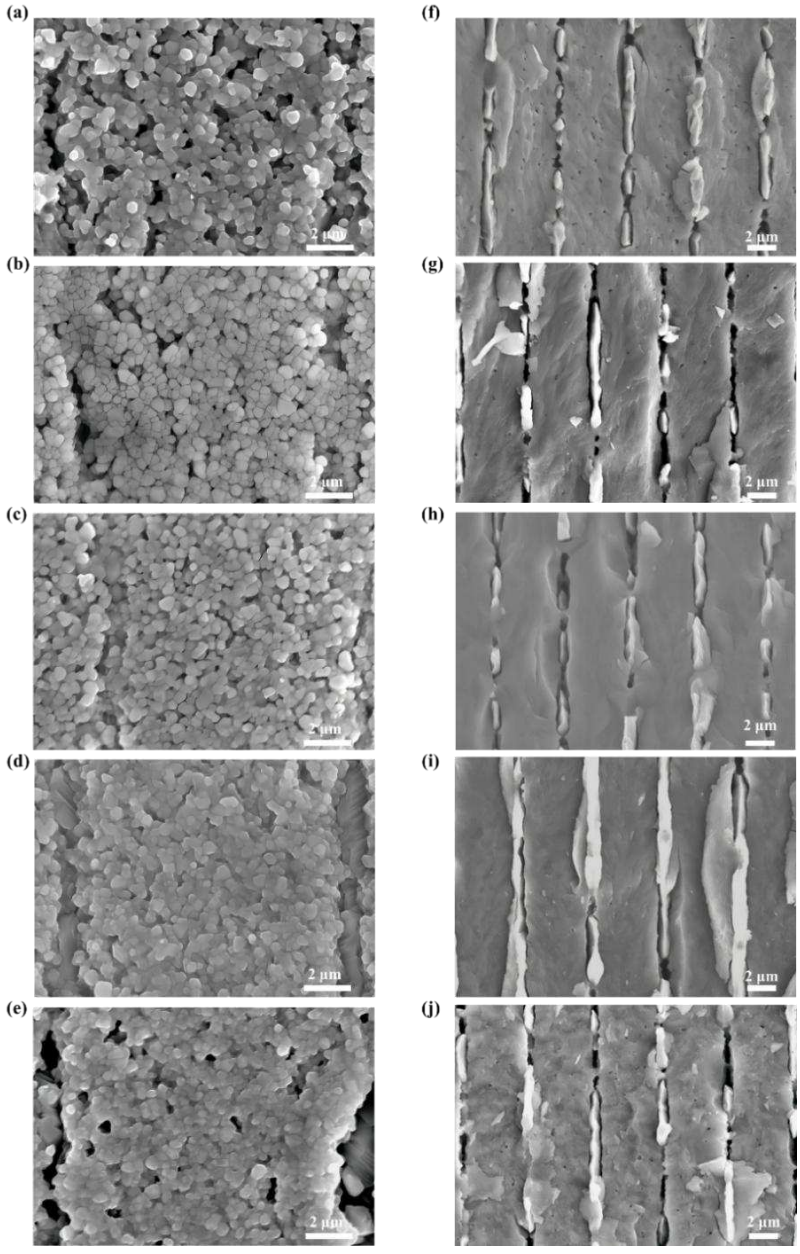


Fig. 4. SEM microstructure diagram of BME-MLCC：(a-e) end-face；(f-j) cross-sectional

Fig. 4(f-j) presented the micro-morphologies of the cross-sections of BME-MLCCs. It was clearly observable that the tiny pores in the dielectric layers of BME-MLCCs in Groups S1-S4 gradually vanished, indicating a significant improvement in compactness. Additionally, it could be found that the continuity of the internal electrodes in BME-MLCCs of Groups S1-S4 gradually became better. As shown in Fig. 1, the ceramic film served as the carrier for the internal electrodes, and its flatness and compactness in micro-morphology played a crucial role in the continuity and shrinkage characteristics of the internal electrodes. From this, it could be seen that the grinding degree not only determined the particle size distribution of BME-MLCCs but also influenced the overall micro-structure of the dielectric layers and internal electrodes.

3.2 Electrical properties

To further investigate the impact of microstructure on the electrical performance of the products, Fig. 5 displayed the test results of five groups of BME-MLCCs. The capacitance values of BME-MLCCs in Groups S1-S5 generally increased step by step numerically, with an anomalous pattern emerging starting from Group S5. Meanwhile, upon examining the capacitance statistical distribution graph, significant differences in the box widths of individual box plots were observed. A narrower box indicated more concentrated data. Based on this, it could be inferred that the capacitances of Groups S1, S2, and S3 were relatively dispersed, while Group S4 had the highest and most stable capacitance values.

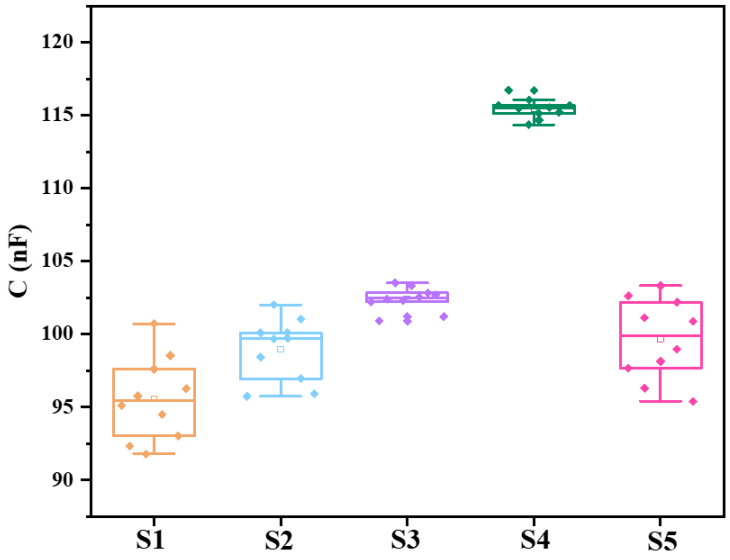


Fig. 5. Statistical Distribution of Capacitance for BME-MLCCs

According to the definition of capacitance, the dielectric constant C be calculated by (equation 1):

$$C = n\frac{\varepsilon s}{4k\pi d} \quad (1)$$

where n is the number of individual capacitors, ε is the dielectric constant, *s* is the efective area of inner electrode, k is the Boltmann constant and *d* is the thickness of individual dielectric layers。Based on the micro-morphologies of the cross-sections of BME-MLCCs, it was evident that there were obvious tiny pores in the dielectric layers both at the initial stage of grinding and after excessive grinding.

According to the effective permittivity theory (EMT) [15], when the medium inside the cavity is air, the dielectric constant is related to the void ratio as follows (equation 2):

$$\frac{\varepsilon_r-1}{\varepsilon_r+2} = (1-P)\cdot\frac{\varepsilon_1-1}{\varepsilon_1+2} \tag{2}$$

ε_r is the dielectric constant of the medium with holes, ε_1 is the dielectric constant of the medium without holes, and *P* is the porosity. It can be seen that the dielectric constant of the sample will decrease when the pore of the sample medium increases. In addition, according to Donhang[16], a multilayer capacitor could be equivalently transformed into the same number of single-layer capacitors connected in parallel. A single-layer capacitor had a capacitance determined by its average grain size (r) and average dielectric thickness (d). The capacitance of a multilayer capacitor was constrained by the grain size and flatness of the single-layer capacitors. From this, it could be inferred that the flatness and size distribution of the dielectric layers played a decisive role in the capacitance dispersion.

Simultaneously, we tested the dielectric loss and insulation resistance (Rj) of the five groups of samples, with results shown in Fig. 6. The insulation resistance of BME-MLCCs in Groups S1-S4 increased significantly, while the dielectric loss gradually decreased. However, a reversal in these trends was seen in Group S5. As grinding degree intensified, the grain size within the dielectric layer decreased, and the number of grain boundaries increased, impeding the propagation of leakage current and thereby enhancing the insulation resistance [17-18]. Additionally, since the ceramic film serves as the carrier for the internal electrodes, its micro-morphology is closely related to the continuity of the internal electrodes and the interfacial bonding strength. Discontinuities in the internal electrodes or interfacial delamination could lead to localized electric field concentration, increasing loss and leakage current, inducing thermal stress cracks, and ultimately compromising insulation performance.

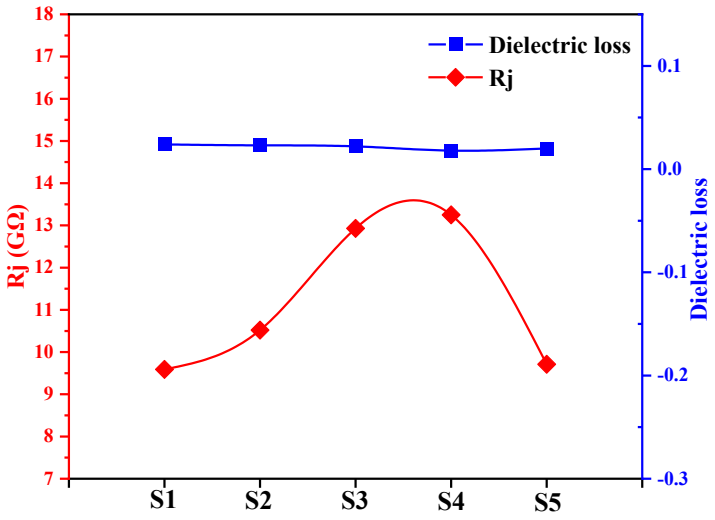


Fig. 6. The dielectric loss and *R*j of BME-MLCC samples with different microstructures

To gain a deeper understanding of the intricate relationship between the microstructure of the dielectric layer and insulation performance, we conducted a residual carbon analysis on the BME-MLCCs from Groups S1 through S5 after the debinding procedure. The results, documented in Table 2, revealed a striking parallelism: the trend of variation in residual carbon content among the five sample groups exhibited a remarkable resemblance to that of the insulation resistance.

According to the diffusion model of organic matter in MLCC proposed by DAS et al [19], the organic matter diffusion coefficient D_{eff} is calculated as (equation 3):

$$D_{\text{eff}} = \frac{\mathrm{D}\beta}{\tau} \tag{3}$$

D is the diffusion coefficient; β is the porosity; τ is the diffusion path. It can be seen that the porcelain body densification and porosity will directly affect the amount of organic matter residue inside the porcelain body. For this reason, through the carbon and sulfur analyzer to test the amount of residual carbon in the sample after debonding, the results are shown in Table 2.

Table 2 The carbon of BME-MLCCs

No.	Grinding time	Carbon (%)	Sample (g)
S1	10	0.37125	0.2024
S2	12	0.34136	0.1906
S3	14	0.27265	0.2045
S4	16	0.22502	0.2113
S5	18	0.31679	0.2043

3.3 Reliability

To thoroughly assess the reliability of the breakdown strength in BME-MLCCs, we utilized the Weibull function to quantitatively evaluate the high-voltage endurance properties and reliability across the five sample groups. The correlation coefficient (Pearson's r) between the breakdown field strength (E) and the Weibull distribution can be calculated by the following (equation 4) [20-21]:

$$\mathrm{p}(E) = 1 - \exp\left[-\left(\frac{E}{E_b}\right)^{\beta}\right] \tag{4}$$

E represented the experimentally measured breakdown values, E_{b} denoted the breakdown strength corresponding to a cumulative failure probability of 63.2%. p(E) stood for the cumulative failure probability, and β was the shape parameter, indicating the degree of dispersion. Fig. 7 displayed the Weibull statistical distribution analysis results obtained by randomly selecting 10 samples from each group. The results revealed that, at room temperature, the E_{b} values for S1, S2, S3, S4, and S5 BME-MLCCs were 361 V/μm, 416 V/μm, 483 V/μm, 494 V/μm, and 384 V/μm, respectively, with corresponding shape parameters of 26.5, 23.4, 41.2, 25.5, and 17.2. All five groups exhibited relatively high shape parameters, indicating the reliability of the Weibull statistical distribution results.

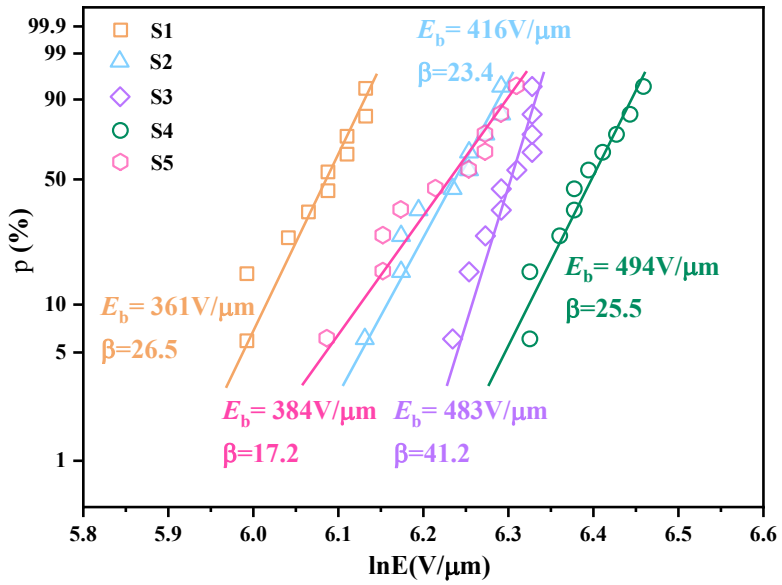


Fig. 7. Weibull distribution plots of breakdown strength for BME-MLCC

Fitting calculations revealed that the breakdown voltage (E_b) of samples rose steadily from Group S1 to S4, then dropped in group S5. Micro-morphological analysis of BME-MLCCs showed non-dense dielectric layers with pores in Groups S1, S2, and S5. Residual carbon tests (Table 2) indicated these pores contained many impurities. These impurities were prone to forming discharge channels under the influence of an electric field [22-23], leading to abnormal increases in local electric field strength and serving as breakdown points, thereby reducing the overall breakdown strength. Research confirmed that non-dense ceramics had lower resistivity and weaker current-blocking ability, allowing easier current penetration and increased charge accumulation, thus raising breakdown likelihood [24-25].

Internal electrode morphology analysis revealed that group S4 had the best electrode continuity and dielectric layer bonding. The other four groups had fractures and gaps in electrodes, where tip effects caused local electric fields to exceed the material's breakdown strength, leading to premature breakdown, localized field concentration, and reduced breakdown voltage.

Therefore, it is necessary to rationally control the microstructure of the ceramic body when preparing capacitors to ensure that they have good breakdown voltage performance.

To further evaluate the impact of microstructure on the lifetime reliability of BME-MLCCs, 40 samples from each of the five groups were subjected to a highly accelerated life test (HALT) [16]. The test conditions were V_2 150 V, V_1 50 V, T_1 and T_2 125 °C. The accelerated life test was stopped when 20 (50%) samples failed. The life failure diagram is shown in Fig. 8. Calculations were performed according to Mogilevsky and Shirn's formula for lifetime (equation 5) [26]:

$$A = \frac{t_1}{t_2} = \left(\frac{V_2}{V_1}\right)^{\alpha} \exp\frac{E_a}{K_B}\left[\frac{1}{T_1} - \frac{1}{T_2}\right] \quad (5)$$

where t is the time, V is the voltage value, T is the temperature (K), E_a is the activation energy (1.3 eV), and K_B is the Boltzmann's constant. α is an empirical parameter related to the type of ceramic and the product model [12]. In the present paper, the empirical parameterα of 3 is used. The results

are shown in Table 3. It can be seen that the samples in group S1 started to fail at the earliest time. Samples in group S4 start to fail the latest, and the failure rate reaches 50% at 292.3 hours, which corresponds to the theoretical lifetimes of 4633.2 hours and 7892.1 hours, respectively.

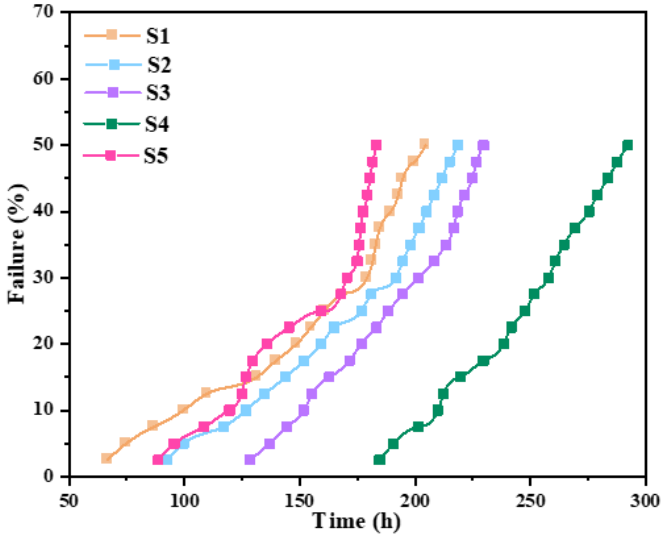


Fig. 8 Weibull distribution of HALT for BME-MLCCs with different microstructures

Table 3. The HALT data of BME-MLCCs with different microstructures

Sample	First failure (h)	Expected life (h)	50% failure (h)	Expected life (h)
S1	54.6	1474.2	204.6	5524.2
S2	84.3	2276.1	218.7	5904.9
S3	112.7	3042.9	229.6	6199.2
S4	171.6	4633.2	292.3	7892.1
S5	74.9	2022.3	183.2	4946.4

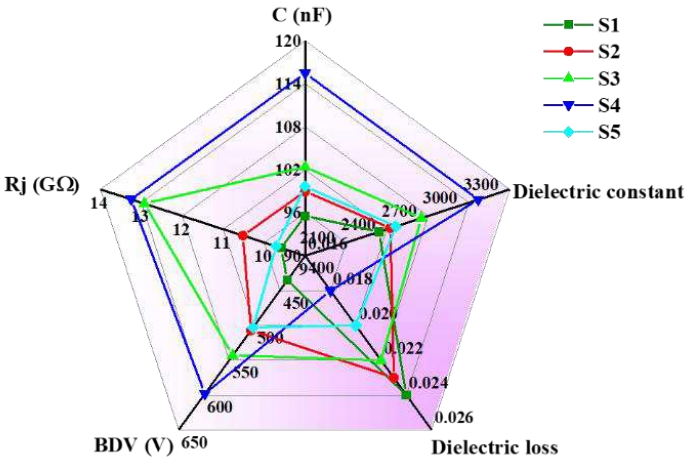


Fig. 9 Radar Chart of Basic Performance for BME-MLCC

Fig. 9 displayed a radar chart that offered a comparative overview of the fundamental performance of BME-MLCCs across various microstructures, with Group S4 emerging as the top performer. Through micro-morphological scrutiny, it became evident that the milling intensity not only governed the particle size within the dielectric layer but also played a pivotal role in determining its density, surface evenness, as well as the continuity of internal electrodes and the robustness of their interfacial bonding. An in-depth analysis of electrical performance underscored a strong linkage between the micro-morphological features of BME-MLCCs and their electrical behavior. Consequently, during the fabrication process of BME-MLCCs, meticulous attention must be devoted to the microstructure at each and every step to safeguard the reliability of the final product.

4. Conclusion

Five types of BME-MLCCs with distinct microstructures were fabricated by adjusting the milling intensity. A comprehensive analysis was conducted to assess the influence of dielectric layer microstructural characteristics-including particle size, density, and surface uniformity-on their electrical performance and reliability. The results indicated that during the initial and final stages of milling, the dielectric layer exhibited suboptimal micro-morphology, resulting in diminished overall performance and reduced reliability. When the milling intensity reached the condition corresponding to Group S4, the dielectric layer achieved an optimal microstructure, characterized by a flat, dense, and pore-free surface, yielding a theoretical lifespan of 7892.1 h.

Funding

No funding was received to assist with the preparation of this manuscript.

CRediT authorship contribution statement

Yunfei He: Conceptualization, Methodology, Investigation, Writing - original draft. Fengju Yi: Validation, Formal analysis, Visualization. Zengwei Zheng: Validation, Formal analysis, Visualization, Writing – review & editing. Qihang Yang: Validation, Formal analysis, – review & editing. Qijun Cheng: Resources, Writing – review & editing, Supervision, Data curation.

Data Availability

Data sharing not applicable to this article as no datasets were generated or analysed during the current study.

Declaration of competing interest

The authors declare that they have no known competing financial interests or personal relationships that could have appeared to influence the work reported in this paper.

References

[1] Wang M, Zhang J, Wang Y, et al (2022) Material and structural design of microsupercapacitors[J]. J. Solid State Electrochem 26(2): 313-334.

[2] Shi Y (2024) Microminiaturization and integration technology of electronic components[J]. Wirel. Internet Sci. Technol 21(13): 11-13.

[3] Zhang L, Li X (2025) Key Electronic Materials: Global Application Progress and Future Development Directions in China[J]. Strateg. Stud. CAE 27(2): 249-268.

[4] Yang Y, Xu K, Yang B, et al (2025) Giant energy storage density with ultrahigh efficiency in multilayer ceramic capacitors via interlaminar strain engineering[J]. Nat. Commun 16(1): 1300.

[5] Chen S, Ding Y, Mu H, et al (2025) Research progress on multilayer ceramic capacitors for energy storage[J]. J. Mater. Sci.:Mater. Electron 36(1): 77.

[6] Yousefian P, Randall C A (2023) Quality assessment and lifetime prediction of base metal electrode multilayer ceramic capacitors: Challenges and opportunities[J]. J. Mater. Sci.:Mater. Electron 6: 100045.

[7] Pattipaka S, Lim Y, Son Y H, et al (2024) Ceramic-based dielectric materials for energy storage capacitor applications[J]. Materials 17(10): 2277.

[8] Yang Q, Cheng Q, Yi F, et al (2025) The influence of varying density of dielectric layer on BME-MLCC[J]. J. Mater. Sci. Mater. Electron 36(1): 47.

[9] Xu X, Gurav A S, Lessner P M, et al (2010) Robust BME class-I MLCCs for harsh-environment applications[J]. IEEE Trans. Ind. Electron 58(7): 2636-2643.

[10] Sohn HY, Moreland C (1968) The effect of particle size distribution on packing density[J]. J. Chem. Eng 46(3): 162-167.

[11] Bierwagen GP, Sanders TE (1974) Studies of the effects of particle size distribution on the packing efficiency of particles[J]. Powder Technol 10(3): 111-119.

[12] Cheng Q, Huang L, Xu H, et al (2019) The influence of particle size of slurry on life on BME‐MLCC[J]. Int. J. Appl. Ceram. Technol 16(4): 1632-1638.

[13] Liu Q, Hao H, Guo QH, et al (2023) Enhanced breakdown strength of $BaTiO_3$-based multilayer ceramic capacitor by structural optimization[J]. Rare Met 42(8): 2552-2561.

[14] Xu P, Guo C, Hao W, et al (2024) Enhancing grain boundary contributions to improve the dielectric properties of $(In_{0.5}Nb_{0.5})_{0.05}Ti_{0.95}O_2$ ceramics by Bi aided sintering[J]. J. Phys. Chem. Solids 187 111881.

[15] Wersing W, Lubitz K, Mohaupt J (1986) Dielectric, elastic and piezoelectric properties of porous PZT ceramics[J]. Ferroelectrics 68(1): 77-97.

[16] Liu D 2014 A general reliability model for Ni-$BaTiO_3$-based multilayer ceramic capacitors[C] Capacitors and Resistors Technology Symposium (CARTS).

[17] Hsiang HI, Yang YH, Huang CY, et al (2023) Dielectric properties of $BaTiO_3$ and $Ba_{0.95}Ca_{0.05}TiO_3$ sintered in a reducing atmosphere[J]. Ceram. Int 49(17): 28751-28757.

[18] Sun F, Zhao H, Miao K (2024) Influence mechanism of Ni_2O_3 doping on leakage current of SnO_2 varistor ceramics[J]. Int. J. Appl. Ceram. Technol 21(5): 3089-3096.

[19] Das A, Madras G, Dasgupta N, et al (2003) Binder removal studies in ceramic thick shapes made by laminated object manufacturing[J]. J. Eur. Ceram. Soc 23(7): 1013-1017.

[20] Wang Y, Chan YC, Gui ZL, et al (1997) Application of Weibull distribution analysis to the dielectric failure of multilayer ceramic capacitors[J]. Mater. Sci. Eng.B 47(3): 197-203.

[21] Yetong LÜ, Yexia QIN, Mei W, et al (2024) The Influence and Mechanism of Grain Size on the Reliability of Multilayer Ceramic Capacitors[J]. J. South China Norm. Univ 56(3): 1-8.

[22] Wenxu J , Yudong H , Mupeng Z ,et al (2018) Advances in lead-free high-temperature dielectric materials for ceramic capacitor application[J]. Iet Nanodielectr 1(1): 3-16.

[23] Jiang J, Yi F, Chen M, et al (2025) Research on Residual Carbon Content and Electrical Properties of Nickel Electrode MLCC After Glue Removal[J]. Electron. Pack 25(1): 10401.

[24] Zhu C, Cai Z, Feng P, et al (2024) Reliability mechanisms of the ultrathin-layered $BaTiO_3$-based BME MLCC[J]. Acta Phys.-Chim 40(1): 2304015.

[25] Weaver P M, Cain M G, Stewart M, et al (2012) The effects of porosity, electrode and barrier materials on the conductivity of piezoelectric ceramics in high humidity and dc electric field[J]. Smart Mater. Struct 21(4): 045012.

[26] Morita K, Shimura T, Abe S, et al (2018) Modified lifetime prediction for multilayer ceramic capacitors based on space charge evolution[J]. Jpn. J. Appl. Phys 57(11S): 11UC03.